Majorana Corner Modes and Flat-Band Majorana Edge Modes in Superconductor/Topological-Insulator/Superconductor Junctions

Xiao-Ting Chen(陈晓婷)[1†], Chun-Hui Liu(刘春晖)[2,3†], Dong-Hui Xu(许东辉)[4,5*], and Chui-Zhen Chen(陈垂针)[1*]

[1]*Institute for Advanced Study and School of Physical Science and Technology, Soochow University, Suzhou 215006, China*
[2]*Beijing National Laboratory for Condensed Matter Physics, Institute of Physics, Chinese Academy of Sciences, Beijing 100190, China*
[3]*School of Physical Sciences, University of Chinese Academy of Sciences, Beijing 100049, China*
[4]*Department of Physics, Chongqing University, Chongqing 400044, China*
[5]*Chongqing Key Laboratory for Strongly Coupled Physics, Chongqing University, Chongqing 400044, China*

(Received 5 June 2023; accepted manuscript online 16 August 2023)

Recently, superconductors with higher-order topology have stimulated extensive attention and research interest. Higher-order topological superconductors exhibit unconventional bulk-boundary correspondence, thus allow exotic lower-dimensional boundary modes, such as Majorana corner and hinge modes. However, higher-order topological superconductivity has yet to be found in naturally occurring materials. We investigate higher-order topology in a two-dimensional Josephson junction comprised of two s-wave superconductors separated by a topological insulator thin film. We find that zero-energy Majorana corner modes, a boundary fingerprint of higher-order topological superconductivity, can be achieved by applying magnetic field. When an in-plane Zeeman field is applied to the system, two corner modes appear in the superconducting junction. Furthermore, we also discover a two-dimensional nodal superconducting phase which supports flat-band Majorana edge modes connecting the bulk nodes. Importantly, we demonstrate that zero-energy Majorana corner modes are stable when increasing the thickness of topological insulator thin film.

DOI: 10.1088/0256-307X/40/9/097403

The search for topological superconductors which host Majorana zero-energy modes has been one of the central subjects in condensed matter physics,[1–6] since they provide an ideal platform to potential applications in quantum computations based on non-Abelian statistics.[7–14] In 2001, Kitaev proposed to realize Majorana zero-energy modes at the ends of one-dimensional p-wave superconductors.[15] Experimentally, the signatures of zero-energy modes were reported to been observed in spin-orbital coupled semiconductor wires in proximity to s-wave superconductors[16–19] and in the vortex of iron-based superconductors.[20–24] However, conclusive identification of Majorana zero energy modes and scalable fabrication of Majorana networks remain challenging.[5,6,25–28]

Recently, higher-order topological phases of matter, such as the higher-order topological insulators and higher-order topological superconductors, have been identified as a novel topological state, which feature the unconventional bulk-boundary correspondence.[29–51] Generally, the nth higher-order topological superconductors in d dimensions support $(d-n)$-dimensional gapless boundary excitations with $2 \leq n \leq d$,[31,52–90] which is in contrast to the d-dimensional conventional topological superconductors with $(d-1)$-dimensional boundary excitations.[1,2,91–93] In this endeavor, Majorana zero-energy modes are supposed to be localized at the corners of a two-dimensional second-order topological superconductor (SOTSC).[31,53–55,58,62,77,80] Due to the fact that naturally occurring topological superconductors are extremely rare, SOTSCs with Majorana Kramers pairs of zero modes or single Majorana zero mode at a corner have been proposed in artificial materials, such as a quantum spin Hall insulators (QSHI) in proximity to a d-wave or an $s_{\pm}$-wave superconductor,[53,54] two coupled chiral p-wave superconductors,[55] Rashba spin-orbit coupled π-junction,[61] etc. However, the experimental implementation remains challenging because of the requirements of ideal helical-edge modes of the QSHI, unconventional superconductivities or complicated junction. Fortunately, topological insulator thin films/s-wave superconductors hybrid structures have been successfully fabricated[94–96] and used to engineer the first-order topological superconductors.[97–99] Even more importantly, a spin-selective Andreev reflection in the vortex of topological insulator/superconductor heterostructure was reported in a scanning tunnel microscope measurement, which is regarded as a fingerprint of Majorana zero-energy modes.[100,101]

In this work, we propose that a topological insulator thin film sandwiched between two s-wave superconductors

†These authors contributed equally to this work.
*Corresponding authors. Email: donghuixu@cqu.edu.cn; czchen@suda.edu.cn
© 2023 Chinese Physical Society and IOP Publishing Ltd

with a phase difference π (see Fig. 1) can realize an SOTSC with two localized Majorana corner modes when applying an in-plane magnetic field. We note that the topological insulator-superconductor sandwich structures have been successfully fabricated in the experiment.[102–104] To be specific, a topological superconducting phase with gapless helical Majorana edge modes is created when the phase difference of the junction is π [see Figs. 2(a) and 2(g)]. Then, the helical Majorana edge modes are gapped out by the in-plane magnetic field due to time-reversal symmetry breaking [see Fig. 2(b)], giving rise to Majorana corner modes [see Figs. 2(e) and 2(h)]. The mechanism of Majorana corners in our proposal is distinguishable from that in Ref. [80]. In Ref. [80], 1D fermionic helical edge modes of quantum spin Hall insulator are firstly gapped by the s-wave pairing, and then an in-plane magnetic field closes and reopens the edge gap to create Majorana corner modes. Moreover, we find that a nodal topological superconducting phase hosting flat-band Majorana edge modes emerges when tuning the magnetic field. We also show that Majorana corner modes exist when varying the number of layers of topological insulator thin film. Our findings make the superconductor-topological-insulator-superconductor junctions an incredibly fertile platform for exploring topological superconducting phase.

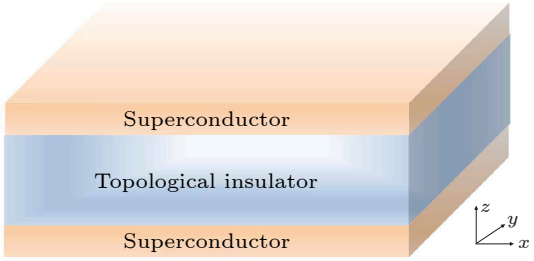

Fig. 1. Schematic diagram of topological insulator multilayer based superconductor junction.

Model Hamiltonian. In reciprocal space, the effective Hamiltonian of the superconductor/topological-insulator/superconductor heterostructure can be written as

$$H(\boldsymbol{k}) = -\frac{A}{a}\sin(k_y a)\sigma_x\tau_z + \frac{A}{a}\sin(k_x a)\rho_z\sigma_y\tau_z + M(\boldsymbol{k})\rho_z\tau_x + \Delta\rho_y\sigma_y\tau_z + V_x\rho_z\sigma_x - \mu\rho_z, \quad (1)$$

in the Nambu basis $C_{\boldsymbol{k}} = (c_{\boldsymbol{k}l,\uparrow}, c_{\boldsymbol{k}l,\downarrow}, c^{\dagger}_{-\boldsymbol{k}l,\uparrow}, c^{\dagger}_{-\boldsymbol{k}l,\downarrow})^{\mathrm{T}}$, where $\uparrow$ and $\downarrow$ represent two electron spin directions, and $l = 1, 2$ is the layer index; σ_i, τ_i and $\rho_i (i = x, y, z)$ are the Pauli matrices. In Eq. (1), they act on the spin, layer, and particle-hole spaces, respectively; σ_0, τ_0 and ρ_0 are the 2×2 identity matrices. $M(\boldsymbol{k}) = m_0 - \frac{2m_1}{a^2}[2 - \cos(k_x a) - \cos(k_y a)]$ describes the mass induced by the hybridization of the top and bottom surfaces of the topological insulator thin film. A is the characteristic parameter of the kinetic energy of the Dirac fermions, and μ denotes the chemical potential. Δ is the s-wave pairing amplitude, and the pairing functions of the top and bottom surfaces of the thin film have opposite sign, which makes the setup a Josephson junction with a π phase shift. V_x represents the in-plane Zeeman field applied along the x direction. We set the lattice constant $a = 5\,\mathrm{nm}$, $A = 300\,\mathrm{meV{\cdot}nm}$ and $m_1 = 150\,\mathrm{meV{\cdot}nm^2}$.[105] For our purpose, we set $m_0 = -2\,\mathrm{meV}$ and $\Delta = 2\,\mathrm{meV}$ in this case.

Before turning to discuss the Majorana corner modes in this junction, we would like to give a brief discussion about the case without applied magnetic field. In this case, time-reversal symmetry restores, a topological superconducting phase with gapless helical Majorana edge modes [see Fig. 2(a)] exists when $m_0^2 < \Delta^2 + \mu^2$.[98] The helical edge modes are confirmed by calculating the Bogoliubov quasiparticle energy spectrum and the local density of states for a square nanodisk, as shown in Figs. 2(d) and 2(g).

Majorana Corner Modes and Flat-Band Edge Modes. When turning on the in-plane Zeeman field, we find that the gapless helical Majorana edge modes are not stable owing to time-reversal symmetry breaking, in the meantime, an energy gap opens as shown in Fig. 2(b). This gap signals the occurrence of the SOTSC. We compute the Bogoliubov quasiparticle spectrum for a finite-sized sample with a rhombus geometry. The spectrum depicted in Fig. 2(e) shows two degenerate Majorana ingap bound states at zero energy, which reside at the top and bottom corners of the rhombus, respectively, as depicted in Fig. 2(h). These two Majorana corner modes are a smoking-gun signature of the SOTSC.

In the following, we will construct a topological invariant and an edge theory based on the Jackiw–Rebbi mechanism to characterize the zero-energy Majorana corner modes in SOTSC phase.

The Hamiltonian maintains the mirror symmetry: $C_{2x}H(k_x, k_y)C_{2x}^{-1} = H(k_x, -k_y)$ with $C_{2x} = i\sigma_x\tau_x$. Along the mirror invariant axis $k_y = 0$ of the first Brillouin zone (BZ), $H(k_x, k_y = 0)$ commutes with C_{2x} operator. We can use a mirror winding number along this axis to characterize the topological properties of the Majorana corner modes.[75,106,107] The expression of $H(k_x, k_y = 0)$ is

$$H(k_x, 0) = \frac{A}{a}\sin(k_x a)\rho_z\sigma_y\tau_z + M(k_x, 0)\rho_z\tau_x + \Delta\rho_y\sigma_y\tau_z + V_x\rho_z\sigma_x - \mu\rho_z, \quad (2)$$

where $M(k_x, 0) = m_0 - \frac{2m_1}{a^2}[1 - \cos(k_x a)]$. C_{2x} has two fourfold degenerate eigenvalues of ± 1. The eigenvectors with eigenvalue of $+1$ are

$$\begin{aligned}\chi_1 &= |\rho_z = 1, \sigma_x = 1, \tau_x = 1\rangle,\\ \chi_2 &= |\rho_z = -1, \sigma_x = 1, \tau_x = 1\rangle,\\ \chi_3 &= |\rho_z = 1, \sigma_x = -1, \tau_x = -1\rangle,\\ \chi_4 &= |\rho_z = -1, \sigma_x = -1, \tau_x = -1\rangle, \end{aligned} \quad (3)$$

which constitutes the $+1$ eigenspace. The eigenvectors with eigenvalue of -1 are

$$\begin{aligned}\chi_5 &= |\rho_z = 1, \sigma_x = 1, \tau_x = -1\rangle,\\ \chi_6 &= |\rho_z = -1, \sigma_x = 1, \tau_x = -1\rangle,\\ \chi_7 &= |\rho_z = 1, \sigma_x = -1, \tau_x = 1\rangle,\\ \chi_8 &= |\rho_z = -1, \sigma_x = -1, \tau_x = 1\rangle, \end{aligned} \quad (4)$$

which constitutes the -1 eigenspace. Projecting $H(k_x, 0)$ into $+1$ eigenspace (-1 eigenspace) of C_{2x}, we can get a

Hamiltonian in the subspace $H_+(k_x,0)$ [$H_-(k_x,0)$]. Using $\chi_1,\chi_2,\ldots,\chi_8$ as a new basis set of Hilbert space, we can get $H(k_x,0)=H_+(k_x,0)\oplus H_-(k_x,0)$ with

$$H_\pm(k_x,0)=\mp\frac{A}{a}\sin(k_x a)\rho_z\sigma_y+M(k_x,0)\rho_z\sigma_z \mp\Delta\rho_y\sigma_y\pm V_x\rho_z\sigma_z-\mu\rho_z. \quad (5)$$

In the first BZ, we can define the Wilson loop operator $W_{\pm,k_x}$ of $H_\pm(k_x,0)$, along the mirror-invariant axis $k_y=0$. The mirror winding number $\nu_\pm$ can be written as [106,107]

$$\nu_\pm=\frac{1}{i\pi}\log(\det[W_{\pm,k_x}])\bmod 2. \quad (6)$$

When corner modes occur, the mirror winding number $\nu_+=\nu_-=1$.[75] The nonzero mirror winding number indicates that the 1D Hamiltonian $H(k_x,0)$ is topological nontrivial with zero energy modes. Alternatively, we can construct an edge theory to understand corner modes,[108] where the Dirac mass domain walls bind zero energy modes. We note that these corner modes are robust when phase shift of the junction is slight deviated from π, which justify the topological robust of the SOTSC. Furthermore, the corner modes are unaffected by the asymmetry of chemical potential and pairing potential of the top and bottom surfaces. See the Supplementary Materials for details.[108]

Continuing to increase the in-plane Zeeman field V_x, we find that the gap closes, and a nodal topological superconducting phase with nodes along the k_y-axis is formed. Considering a ribbon geometry with the open boundary condition along x direction, we plot the energy spectrum in Fig. 2(c). Clearly, this nodal phase hosts flat-band Majorana edge modes in between the two bulk nodes. The flat-band Majorana edge modes are confirmed by calculating the energy spectrum and the local density of states of the edge modes, as displayed in Figs. 2(f) and 2(i). We can see that the flat-band Majorana edge modes are located on the top and bottom edges of the sample. The Majorana flat band is featured by a quantized zero-bias conductance peak $2Ne^2/h$ in transport measurement, where N is the number of Majorana zero modes in the Majorana flat band.[109] We note that the Majorana flat band will be tilted,[110] if the paring potential Δ and chemical potential μ on the top and bottom surfaces are different. To realize symmetric parameters, we can use highly gate tunable two-dimensional superconductors MoS_2 and $NbSe_2$[111,112] to avoid the electrostatic screening by the superconductors.

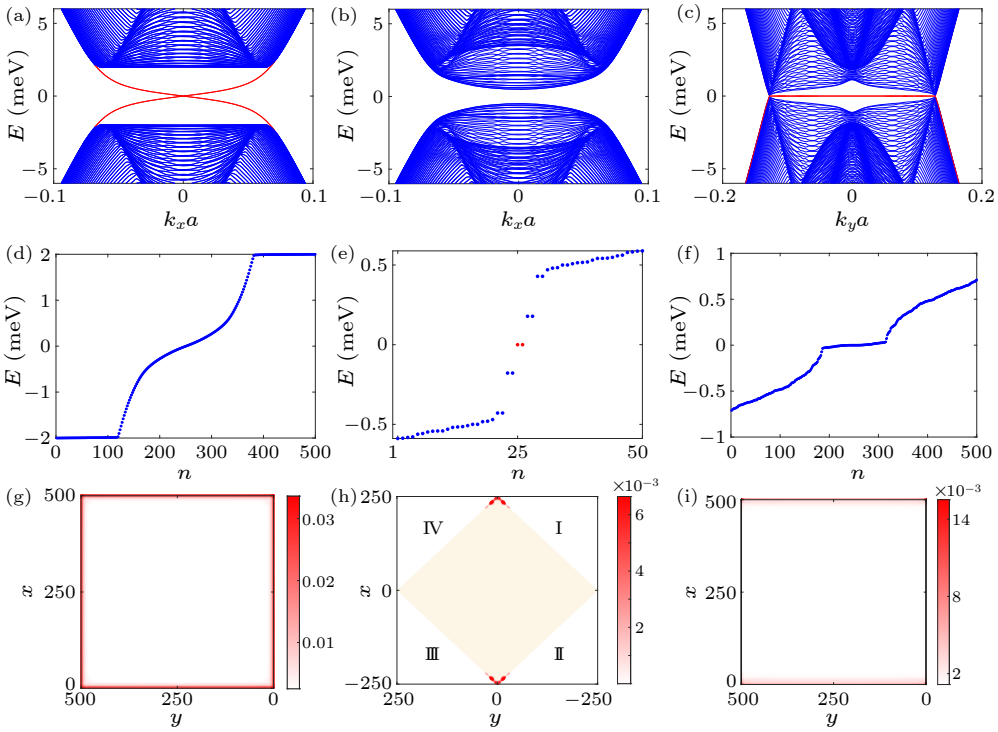

Fig. 2. Energy dispersions of nanoribbons geometry along x direction for (a) $V_x=0$ meV, (b) $V_x=1.5$ meV, and along y direction for (c) $V_x=12$ meV. Correspondingly, (d)–(f) the energy spectrum and (g)–(i) local density states, for the sample configurations shown in (g)–(i), where model parameters are the same as those in (a)–(c), respectively. Other parameters are $\mu=12$ meV and $\Delta=2$ meV.

To capture the topological characteristic of the nodal phase, we further adopt the Wilson loop method[32,33,37,113–116] to calculate the bulk polarization of the system. Since the bulk nodes are located along the k_y-axis, by treating k_y as a parameter, the effective Hamiltonian reduces to a one-dimensional Hamiltonian $H_{k_x}(k_y)$. The Wilson loop operator[32,33,37,113–116] along the path in the k_x-direction W_{x,k_x} is defined by $W_{x,k_x}=F_{x,k_x+(N_x-1)\Delta k_x}\cdots F_{x,k_x+\Delta k_x}F_{x,k_x}$, where k_x is the base point and N_x is the number of unit cells in the x-direction. Here, $[F_{x,k_x}]^{mn}=\langle u^m_{k_x+\Delta k_x}|u^n_{k_x}\rangle$ with the step $\Delta k_x=2\pi/N_x$, and $|u^n_{k_x}\rangle$ represents the occupied Bloch

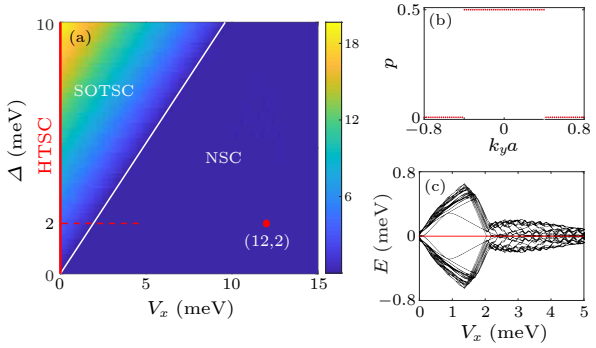

Fig. 3. (a) Phase diagram of topological superconductors. The upper left regime marked by SOTSC represents the second-order topological superconductor phase. The lower right regime marked by NSC (nodal topological superconductor) represents the nodal topological superconductor phase. The left red solid line represents the helical topological superconductor (HTSC) phase in the absence of V_x. The color bar represents the energy gap. (b) Bulk polarization of the nodal phase as a function of k_y. In (a) and (b), we fix $\mu = 12\,\text{meV}$. In (b), we also fix $\Delta_t = 2\,\text{meV}$ and $V_x = 12\,\text{meV}$. (c) Energy spectrum as a function of V_x for a finite-sized sample with rhombus geometry. The parameters correspond to the red dashed line in (a).

wave functions with $n = 1, 2, \ldots, N_{\text{occ}}$. $N_{\text{occ}} = N_b/2$ is the number of occupied bands, with N_b the degrees of freedom for each cell. Fixing k_y, we can determine the Wilson loop operator W_{x,k_x} on a path along k_x. The Wannier center v_x^j can be determined by the eigenvalues of the Wilson-loop operator W_{x,k_x},

$$W_{x,k_x}|v^j_{x,k_x}\rangle = e^{i2\pi v_x^j}|v^j_{x,k_x}\rangle, \tag{7}$$

where $j \in \{1, 2, \ldots, N_{\text{occ}}\}$ labels eigenstates $|v^j_{x,k_x}\rangle$ as well as components $[v^j_{x,k_x}]^n$. Since k_y is fixed, the bulk polarization can be define as $p = \sum_j v_x^j \bmod 1$.[32] We plot the bulk polarization as a function of k_y as shown in Fig. 3(b). It is clear that the polarization is quantized to 1/2 between two nodal points. We remark that the topological characteristic of the nodal phase can be portrayed by the k_y-dependent polarization.

Finally, we plot the topological superconducting phase diagram on the plane of Δ and V_x as shown in Fig. 3(a). The phase boundaries are determined by numerically observing the gap closure of the bulk. The phase boundary between SOTSC and the nodal topological superconductor (NSC) is approximately fitted by the line $V_x = \Delta$. By tuning the in-plane Zeeman field V_x, SOTSC phase, NSC phase, and helical topological superconductor (HTSC) phase can be achieved. Figure 3(c) shows the energy spectrum as a function of V_x for the finite-sized sample with rhombus-like geometry in Fig. 2(h).

The effect of thickness on Majorana corner modes. Here, we study how the thickness of the topological insulator thin film affects the Majorana corner modes. In the three-dimensional limit, the bulk Hamiltonian of the intermediate topological insulator can be expressed as

$$\begin{aligned} H_{\text{3DTI}}(\boldsymbol{k}) = {} & \frac{A}{a}\sin(k_x a)\sigma_x\tau_x + \frac{A}{a}\sin(k_y a)\sigma_y\tau_x - \mu \\ & + \frac{A}{a}\sin(k_z a)\sigma_z\tau_x + M(\boldsymbol{k})\tau_z + V_x\sigma_x, \end{aligned} \tag{8}$$

where $M(\boldsymbol{k}) = m_0 - 2\frac{t_x}{a^2}[1-\cos(k_x a)] - 2\frac{t_y}{a^2}[1-\cos(k_y a)] - 2\frac{t_z}{a^2}[1-\cos(k_z a)]$ with $\boldsymbol{k} = (k_x, k_y, k_z)$, and V_x is the Zeeman field along the x-direction.

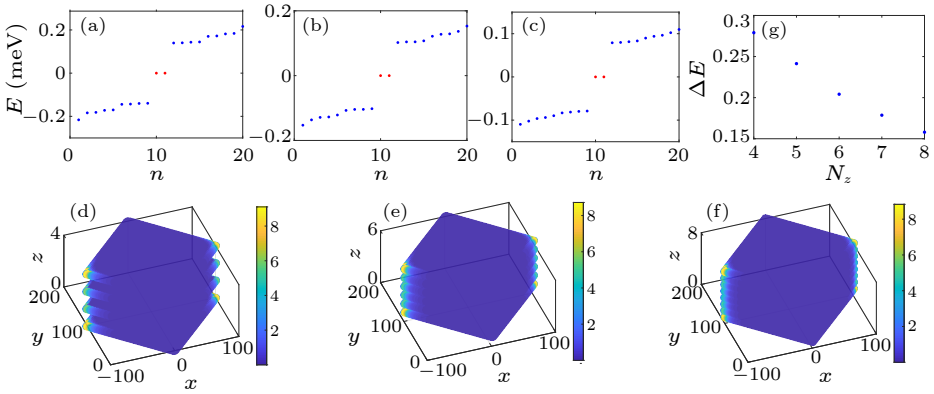

Fig. 4. $N_x \times N_y = 200 \times 200$ and rhombus-shaped sample for all plots. The energy spectrum for distinct numbers of layers: (a) $N_z = 4$, (b) $N_z = 6$, and (c) $N_z = 8$. Here (d), (e), and (f) are the local density of the two Majorana ingap bound states marked in red dots in (a), (b), and (c), respectively. (g) The gap of bulk spectrum marked in blue dots as a function of number of layers N_z. In (a)–(g), we set $a = 5\,\text{nm}$, $A = 50\,\text{meV·nm}$, $m_0 = 8\,\text{meV}$, $\mu = 2\,\text{meV}$, $\Delta = 2\,\text{meV}$, $V_x = 1.5\,\text{meV}$, $t_x = t_y = 125\,\text{meV·nm}^2$, and $t_z = 100\,\text{meV·nm}^2$.

For simplicity, we consider that the proximity-induced superconducting gap only exits on outermost layers of the top and bottom surfaces of the three-dimensional topological insulator, and the top and bottom superconductors remain a π phase shift. In reality, the proximity-induced superconducting potential decreases exponentially and can extend to several layers.[94,96] However, this will not change the physics discussed here. Considering the confinement of the topological insulator thin film along the z-direction, the total Hamiltonian in the Nambu space can be written as

$$H_{\text{3D}}(\boldsymbol{k}_\parallel) = \sum_{z=1}^{N_z-1} b^\dagger_{\boldsymbol{k}_\parallel,z}\Big(-\frac{iA}{2}\sigma_z\tau_x + t_z\rho_z\tau_z\Big)b_{\boldsymbol{k}_\parallel,z+1} + \text{h.c.}$$

$$+\sum_{z=1}^{N_z} b^{\dagger}_{\boldsymbol{k}_\parallel,z}[A\sin(k_x a)\sigma_x\tau_x + A\sin(k_y a)\rho_z\sigma_y\tau_x + V_x\rho_z\sigma_x - \mu\rho_z + \tilde{M}(\boldsymbol{k}_\parallel)\rho_z\tau_z]b_{\boldsymbol{k}_\parallel,z} + (b^{\dagger}_{\boldsymbol{k}_\parallel,1}\Delta\rho_y\sigma_y b_{\boldsymbol{k}_\parallel,1} - b^{\dagger}_{\boldsymbol{k}_\parallel,N_z}\Delta\rho_y\sigma_y b_{\boldsymbol{k}_\parallel,N_z}), \quad (9)$$

where $b_{\boldsymbol{k}_\parallel,z} = [\psi_{l,\alpha}(\boldsymbol{k}_\parallel,z), \psi^{\dagger}_{l,\alpha}(-\boldsymbol{k}_\parallel,z)]^{\mathrm{T}}$ with the orbital index $l = P1(P2)$ and the spin index $\alpha = \uparrow(\downarrow)$. $\tilde{M}(\boldsymbol{k}_\parallel) = m_0 - 2t_x(1-\cos(k_x a)) - 2t_y(1-\cos(k_y a)) - 2t_z/a^2$ and $\boldsymbol{k}_\parallel = (k_x, k_y)$. Generally, the low energy physics of the topological insulator thin film $H_{3\mathrm{D}}(\boldsymbol{k}_\parallel)$ can be described by the 2D Hamiltonian $H(\boldsymbol{k})$ in Eq. (1).[117] Similar to $H(\boldsymbol{k})$, the Hamiltonian $H_{3\mathrm{D}}(\boldsymbol{k}_\parallel)$ preserves the mirror-like symmetry: $C_{2x}H_{3\mathrm{D}}(k_x,k_y)C^{-1}_{2x} = H_{3\mathrm{D}}(k_x,-k_y)$ with $C_{2x} = i\sigma_x\mathcal{U}$. Here $N_z\times N_z$ antidiagonal matrix $\mathcal{U}_{ij} = \delta_{i+j,N_z+1}$ is defined in real space with Kronecker delta $\delta_{i,j}$. Therefore, it is natural to expect that the Majorana corner modes will be sustainable with the varying thickness. For $\Delta \neq 0$, $V_x = 0$, the system is a helical topological superconductor, if the Fermi energy is outside the surface gap.[98] By turning on the Zeeman field $V_x > 0$, the gapless Majorana corner modes are observed, as shown in Fig. 4. Figures 4(a), 4(b), and 4(c) show the energy spectrum (only the 20 eigenenergies with the smallest absolute value are shown) of an $N_x\times N_y = 200\times 200$ rhombus-shaped sample. Again, two zero-energy ingap Majorana bound states appear (marked by the red dots in Fig. 4). Figures 4(d), 4(e), and 4(f) are the local density of the two zero-energy Majorana bound states in Figs. 4(a), 4(b), and 4(c), respectively. We can see that the two Majorana bound states are also localized at two opposite corners in the xy-plane, but extended in hinge of the side surface along the z-direction. In order to explore the relationship between the gap of side-surface spectrum [marked in blue dots in Figs. 4(a)–4(c)] and the number of layers N_z, we plot the band gap for different numbers of layers N_z in Fig. 4(g). The band gap decreases rapidly with the increase of N_z due to the decreasing finite-size confinement along the z-direction.

In conclusion, we have illustrated that an SOTSC with two Majorana corner modes is realized in topological insulator thin film based superconducting junctions with a π phase shift when an in-plane Zeeman field is applied. We employ the mirror winding number to characterize the second-order topology of Majorana corner modes. We also analytically deduce an edge theory for the Majorana corner modes by using the perturbation theory. By tuning the Zeeman field, we also observe a nodal superconducting phase hosting flat-band Majorana edge modes, whose bulk topology can be captured by a k-dependent polarization. Lastly, we demonstrate how the thickness of topological insulator thin films affects the Majorana corner modes and their spatial distribution.

Acknowledgement. This work was supported by the National Natural Science Foundation of China (Grant Nos. 12074108, 11974256, and 12147102), the Priority Academic Program Development (PAPD) of Jiangsu Higher Education Institution, and the Natural Science Foundation of Chongqing (Grant No. CSTB2022NSCQ-MSX0568).

References

[1] Hasan M Z and Kane C L 2010 *Rev. Mod. Phys.* **82** 3045
[2] Qi X L and Zhang S C 2011 *Rev. Mod. Phys.* **83** 1057
[3] Alicea J 2012 *Rep. Progress Physics* **75** 076501
[4] Beenakker C 2013 *Annu. Rev. Condens. Matter Phys.* **4** 113
[5] Lutchyn R M, Bakkers E P, Kouwenhoven L P, Krogstrup P, Marcus C M, and Oreg Y 2018 *Nat. Rev. Mater.* **3** 52
[6] Flensberg K, von Oppen F, and Stern A 2021 *Nat. Rev. Mater.* **6** 944
[7] Ivanov D A 2001 *Phys. Rev. Lett.* **86** 268
[8] Kitaev A Y 2003 *Ann. Phys.* **303** 2
[9] Nayak C, Simon S H, Stern A, Freedman M, and Das S S 2008 *Rev. Mod. Phys.* **80** 1083
[10] Alicea J, Oreg Y, Refael G, von Oppen F, and Fisher M P A 2011 *Nat. Phys.* **7** 412
[11] Flensberg K 2011 *Phys. Rev. Lett.* **106** 090503
[12] van Heck B, Akhmerov A R, Hassler F, Burrello M, and Beenakker C W J 2012 *New J. Phys.* **14** 035019
[13] Aasen D, Hell M, Mishmash R V, Higginbotham A, Danon J, Leijnse M, Jespersen T S, Folk J A, Marcus C M, Flensberg K, and Alicea J 2016 *Phys. Rev. X* **6** 031016
[14] Shao L B, Wang Z D, Shen R, Sheng L, Wang B G, and Xing D Y 2017 *Chin. Phys. Lett.* **34** 067401
[15] Kitaev A Y 2001 *Phys. Usp.* **44** 131
[16] Mourik V, Zuo K, Frolov S M, Plissard S R, Bakkers E P A M, and Kouwenhoven L P 2012 *Science* **336** 1003
[17] Das A, Ronen Y, Most Y, Oreg Y, Heiblum M, and Shtrikman H 2012 *Nat. Phys.* **8** 887
[18] Deng M T, Yu C L, Huang G Y, Larsson M, Caroff P, and Xu H Q 2012 *Nano Lett.* **12** 6414
[19] Lutchyn R M, Sau J D, and Das S S 2010 *Phys. Rev. Lett.* **105** 077001
[20] Zhang P, Yaji K, Hashimoto T, Ota Y, Kondo T, Okazaki K, Wang Z, Wen J, Gu G D, Ding H, and Shin S 2018 *Science* **360** 182
[21] Kong L Y, Zhu S Y, Papaj M, Chen H, Cao L, Isobe H, Xing Y, Liu W, Wang D, Fan P, Sun Y, Du S, Schneeloch J, Zhong R, Gu G, Fu L, Gao H J, and Ding H 2019 *Nat. Phys.* **15** 1181
[22] Wang D F, Kong L Y, Fan P, Chen H, Zhu S Y, Liu W Y, Cao L, Sun Y J, Du S X, Schneeloch J, Zhong R D, Gu G D, Fu L, Ding H, and Gao H J 2018 *Science* **362** 333
[23] Liu Q, Chen C, Zhang T, Peng R, Yan Y J, Wen C H P, Lou X, Huang Y L, Tian J P, Dong X L, Wang G W, Bao W C, Wang Q H, Yin Z P, Zhao Z X, and Feng D L 2018 *Phys. Rev. X* **8** 041056
[24] Zhu S Y, Kong L Y, Cao L, Chen H, Papaj M, Du S, Xing Y Q, Liu W Y, Wang D F, Shen C M *et al.* 2020 *Science* **367** 189
[25] Karzig T, Knapp C, Lutchyn R M, Bonderson P, Hastings M B, Nayak C, Alicea J, Flensberg K, Plugge S, Oreg Y, Marcus C M, and Freedman M H 2017 *Phys. Rev. B* **95** 235305
[26] Chen C, Liu Q, Zhang T Z, Li D, Shen P P, Dong X L, Zhao Z X, Zhang T, and Feng D L 2019 *Chin. Phys. Lett.* **36** 057403
[27] Liu S, Nie S M, Qi Y P, Guo Y F, Yuan H T, Yang L X, Chen Y L, Wang M X, and Liu Z K 2021 *Chin. Phys. Lett.* **38** 077302
[28] Pan D, Song H, Zhang S, Liu L, Wen L, Liao D, Zhuo R, Wang Z, Zhang Z, Yang S, Ying J, Miao W, Shang R, Zhang H, and Zhao J 2022 *Chin. Phys. Lett.* **39** 058101
[29] Peng Y, Bao Y, and von Oppen F 2017 *Phys. Rev. B* **95** 235143
[30] Song Z D, Fang Z, and Fang C 2017 *Phys. Rev. Lett.* **119** 246402
[31] Langbehn J, Peng Y, Trifunovic L, von Oppen F, and Brouwer P W 2017 *Phys. Rev. Lett.* **119** 246401
[32] Benalcazar W A, Bernevig B A, and Hughes T L 2017 *Phys. Rev. B* **96** 245115
[33] Benalcazar W A, Bernevig B A, and Hughes T L 2017 *Science* **357** 61

[34] Schindler F, Cook A M, Vergniory M G, Wang Z, Parkin S S, Bernevig B A, and Neupert T 2018 *Sci. Advances* **4** eaat0346
[35] van Miert G and Ortix C 2018 *Phys. Rev. B* **98** 081110
[36] Ezawa M 2018 *Phys. Rev. B* **97** 241402
[37] Franca S, van den Brink J, and Fulga I C 2018 *Phys. Rev. B* **98** 201114
[38] Ezawa M 2018 *Phys. Rev. B* **97** 155305
[39] Ezawa M 2018 *Phys. Rev. Lett.* **120** 026801
[40] Ezawa M 2018 *Phys. Rev. Lett.* **121** 116801
[41] Kunst F K, van Miert G, and Bergholtz E J 2018 *Phys. Rev. B* **97** 241405
[42] You Y Z, Devakul T, Burnell F J, and Neupert T 2018 *Phys. Rev. B* **98** 235102
[43] Wang Z J, Wieder B J, Li J, Yan B, and Bernevig B A 2019 *Phys. Rev. Lett.* **123** 186401
[44] Kudo K, Yoshida T, and Hatsugai Y 2019 *Phys. Rev. Lett.* **123** 196402
[45] Trifunovic L and Brouwer P W 2019 *Phys. Rev. X* **9** 011012
[46] Yue C M, Xu Y F, Song Z D, Weng H M, Lu Y M, Fang C, and Dai X 2019 *Nat. Phys.* **15** 577
[47] Xu Y F, Song Z D, Wang Z J, Weng H M, and Dai X 2019 *Phys. Rev. Lett.* **122** 256402
[48] Hua C B, Chen R, Zhou B, and Xu D H 2020 *Phys. Rev. B* **102** 241102
[49] Chen R, Chen C Z, Gao J H, Zhou B, and Xu D H 2020 *Phys. Rev. Lett.* **124** 036803
[50] Rasmussen A and Lu Y M 2020 *Phys. Rev. B* **101** 085137
[51] Han B, Zeng J, and Qiao Z 2022 *Chin. Phys. Lett.* **39** 017302
[52] Geier M, Trifunovic L, Hoskam M, and Brouwer P W 2018 *Phys. Rev. B* **97** 205135
[53] Yan Z G, Song F, and Wang Z 2018 *Phys. Rev. Lett.* **121** 096803
[54] Wang Q Y, Liu C C, Lu Y M, and Zhang F 2018 *Phys. Rev. Lett.* **121** 186801
[55] Zhu X Y 2018 *Phys. Rev. B* **97** 205134
[56] Khalaf E 2018 *Phys. Rev. B* **97** 205136
[57] Wang Y X, Lin M, and Hughes T L 2018 *Phys. Rev. B* **98** 165144
[58] Liu T, He J J, and Nori F 2018 *Phys. Rev. B* **98** 245413
[59] Hsu C H, Stano P, Klinovaja J, and Loss D 2018 *Phys. Rev. Lett.* **121** 196801
[60] Shapourian H, Wang Y, and Ryu S 2018 *Phys. Rev. B* **97** 094508
[61] Volpez Y, Loss D, and Klinovaja J 2019 *Phys. Rev. Lett.* **122** 126402
[62] Pan X H, Yang K J, Chen L, Xu G, Liu C X, and Liu X 2019 *Phys. Rev. Lett.* **123** 156801
[63] Franca S, Efremov D V, and Fulga I C 2019 *Phys. Rev. B* **100** 075415
[64] Varjas D, Lau A, Pöyhönen K, Akhmerov A R, Pikulin D I, and Fulga I C 2019 *Phys. Rev. Lett.* **123** 196401
[65] Yan Z G 2019 *Phys. Rev. Lett.* **123** 177001
[66] Laubscher K, Chughtai D, Loss D, and Klinovaja J 2020 *Phys. Rev. B* **102** 195401
[67] Zeng C C, Stanescu T D, Zhang C W, Scarola V W, and Tewari S 2019 *Phys. Rev. Lett.* **123** 060402
[68] Zhu X Y 2019 *Phys. Rev. Lett.* **122** 236401
[69] Bultinck N, Bernevig B A, and Zaletel M P 2019 *Phys. Rev. B* **99** 125149
[70] Zhang R X, Cole W S, and Das S S 2019 *Phys. Rev. Lett.* **122** 187001
[71] Zhang R X, Cole W S, Wu X, and Das S S 2019 *Phys. Rev. Lett.* **123** 167001
[72] Wu Z, Yan Z, and Huang W 2019 *Phys. Rev. B* **99** 020508
[73] Ghorashi S A A, Hu X, Hughes T L, and Rossi E 2019 *Phys. Rev. B* **100** 020509
[74] Yan Z 2019 *Phys. Rev. B* **100** 205406
[75] Liu Z R, Hu L H, Chen C Z, Zhou B, and Xu D H 2021 *Phys. Rev. B* **103** L201115
[76] Hsu Y T, Cole W S, Zhang R X, and Sau J D 2020 *Phys. Rev. Lett.* **125** 097001
[77] Wu X X, Benalcazar W A, Li Y, Thomale R, Liu C X, and Hu J 2020 *Phys. Rev. X* **10** 041014
[78] Kheirkhah M, Yan Z, Nagai Y, and Marsiglio F 2020 *Phys. Rev. Lett.* **125** 017001
[79] Laubscher K, Loss D, and Klinovaja J 2020 *Phys. Rev. Res.* **2** 013330
[80] Wu Y J, Hou J, Li Y M, Luo X W, Shi X, and Zhang C 2020 *Phys. Rev. Lett.* **124** 227001
[81] Ahn J and Yang B J 2020 *Phys. Rev. Res.* **2** 012060
[82] Roy B 2020 *Phys. Rev. B* **101** 220506
[83] Ghorashi S A A, Hughes T L, and Rossi E 2020 *Phys. Rev. Lett.* **125** 037001
[84] Tiwari A, Jahin A, and Wang Y 2020 *Phys. Rev. Res.* **2** 043300
[85] Fu B, Hu Z A, Li C A, Li J, and Shen S Q 2021 *Phys. Rev. B* **103** L180504
[86] Kheirkhah M, Nagai Y, Chen C, and Marsiglio F 2020 *Phys. Rev. B* **101** 104502
[87] Ikegaya S, Rui W B, Manske D, and Schnyder A P 2021 *Phys. Rev. Res.* **3** 023007
[88] Roy B and Juričić V 2021 *Phys. Rev. B* **104** L180503
[89] Qin S, Fang C, Zhang F C, and Hu J 2022 *Phys. Rev. X* **12** 011030
[90] Scammell H D, Ingham J, Geier M, and Li T 2022 *Phys. Rev. B* **105** 195149
[91] Shen S Q 2012 *Topological Insulators* (Berlin: Springer)
[92] Bernevig B A 2013 *Topological Insulators and Topological Superconductors* (New Jersey: Princeton University Press)
[93] Zhang R X and Das S S 2021 *Phys. Rev. Lett.* **126** 137001
[94] Wang M X, Liu C, Xu J P, Yang F, Miao L, Yao M Y, Gao C, Shen C, Ma X, Chen X *et al.* 2012 *Science* **336** 52
[95] Xu S Y, Alidoust N, Belopolski I *et al.* 2014 *Nat. Phys.* **10** 943
[96] Xu J P, Liu C, Wang M X, Ge J, Liu Z L, Yang X, Chen Y, Liu Y, Xu Z A, Gao C L, Qian D, Zhang F C, and Jia J F 2014 *Phys. Rev. Lett.* **112** 217001
[97] Fu L and Kane C L 2008 *Phys. Rev. Lett.* **100** 096407
[98] Liu C X and Trauzettel B 2011 *Phys. Rev. B* **83** 220510
[99] Oshima D, Ikegaya S, Schnyder A P, and Tanaka Y 2022 *Phys. Rev. Res.* **4** L022051
[100] Sun H H, Zhang K W, Hu L H, Li C, Wang G Y, Ma H Y, Xu Z A, Gao C L, Guan D D, Li Y Y, Liu C, Qian D, Zhou Y, Fu L, Li S C, Zhang F C, and Jia J F 2016 *Phys. Rev. Lett.* **116** 257003
[101] Shang X, Liu H W, and Xia K 2019 *Chin. Phys. Lett.* **36** 107102
[102] Qu F, Yang F, Shen J, Ding Y, Chen J, Ji Z, Liu G, Fan J, Jing X, Yang C, and Lu L 2012 *Sci. Rep.* **2** 339
[103] Zhang H, Ma X, Li L, Langenberg D, Zeng C G, and Miao G X 2018 *J. Mater. Res.* **33** 2423
[104] Zhang X, Lyu Z, Yang G, Li B, Hou Y L, Le T, Wang X, Wang A, Sun X, Zhuo E, Liu G, Shen J, Qu F, and Lu L 2022 *Chin. Phys. Lett.* **39** 017401
[105] Zhang Y, He K, Chang C Z, Song C L, Wang L L, Chen X, Jia J F, Fang Z, Dai X, Shan W Y, Shen S Q, Niu Q, Qi X L, Zhang S C, Ma X C, and Xue Q K 2010 *Nat. Phys.* **6** 712
[106] Park M J, Kim Y, Cho G Y, and Lee S 2019 *Phys. Rev. Lett.* **123** 216803
[107] Liu T, Zhang Y R, Ai Q, Gong Z, Kawabata K, Ueda M, and Nori F 2019 *Phys. Rev. Lett.* **122** 076801
[108] See Supplementary materials for detail discussion about edge theory, phase effect and asymmetric.
[109] Yuan N F Q, Lu Y, He J J, and Law K T 2017 *Phys. Rev. B* **95** 195102
[110] Wong C L M and Law K T 2012 *Phys. Rev. B* **86** 184516
[111] Lu J M, Zheliuk O, Leermakers I, Yuan N F Q, Zeitler U, Law K T, and Ye J T 2015 *Science* **350** 1353
[112] Xi X, Wang Z, Zhao W, Park J H, Law K T, Berger H, Forró L, Shan J, and Mak K F 2016 *Nat. Phys.* **12** 139
[113] Berry M V 1984 *Proc. R. Soc. London A* **392** 45
[114] Wilczek F and Zee A 1984 *Phys. Rev. Lett.* **52** 2111
[115] Alexandradinata A, Dai X, and Bernevig B A 2014 *Phys. Rev. B* **89** 155114
[116] Luo X W and Zhang C 2019 *Phys. Rev. Lett.* **123** 073601
[117] Liu C X, Zhang H, Yan B, Qi X L, Frauenheim T, Dai X, Fang Z, and Zhang S C 2010 *Phys. Rev. B* **81** 041307